• Retracted •

Mutations in *CLCN2* encoding a voltage-gated chloride channel are associated with idiopathic generalized epilepsies

Karsten Haug[1*], Maike Warnstedt[2*], Alexi K. Alekov[3*], Thomas Sander[4], Alfredo Ramírez[1], Barbara Poser[2], Snezana Maljevic[3], Simon Hebeisen[2], Christian Kubisch[1], Johannes Rebstock[5], Steve Horvath[6], Kerstin Hallmann[1], Joern S. Dullinger[1], Birgit Rau[1], Fritz Haverkamp[7], Stefan Beyenburg[5], Herbert Schulz[4], Dieter Janz[4], Bernd Giese[8], Gerhard Müller-Newen[8], Peter Propping[1], Christian E. Elger[5], Christoph Fahlke[2,9*], Holger Lerche[3*] & Armin Heils[1,5*]

These authors contributed equally to this work.

Published online 3 March 2003, doi:10.1038/ng1121

Idiopathic generalized epilepsy (IGE) is an inherited neurological disorder affecting about 0.4% of the world's population. Mutations in ten genes causing distinct forms of idiopathic epilepsy have been identified so far[1–7], but the genetic basis of many IGE subtypes is still unknown. Here we report a gene associated with the four most common IGE subtypes: childhood and juvenile absence epilepsy (CAE and JAE), juvenile myoclonic epilepsy (JME), and epilepsy with grand mal seizures on awakening (EGMA; ref. 8). We identified three different heterozygous mutations in the chloride-channel gene *CLCN2* in three unrelated families with IGE. These mutations result in (i) a premature stop codon (M200fsX231), (ii) an atypical splicing (del74–117) and (iii) a single amino-acid substitution (G715E). All mutations produce functional alterations that provide distinct explanations for their pathogenic phenotypes. M200fsX231 and del74–117 cause a loss of function of ClC-2 channels and are expected to lower the transmembrane chloride gradient essential for GABAergic inhibition. G715E alters voltage-dependent gating, which may cause membrane depolarization and hyperexcitability.

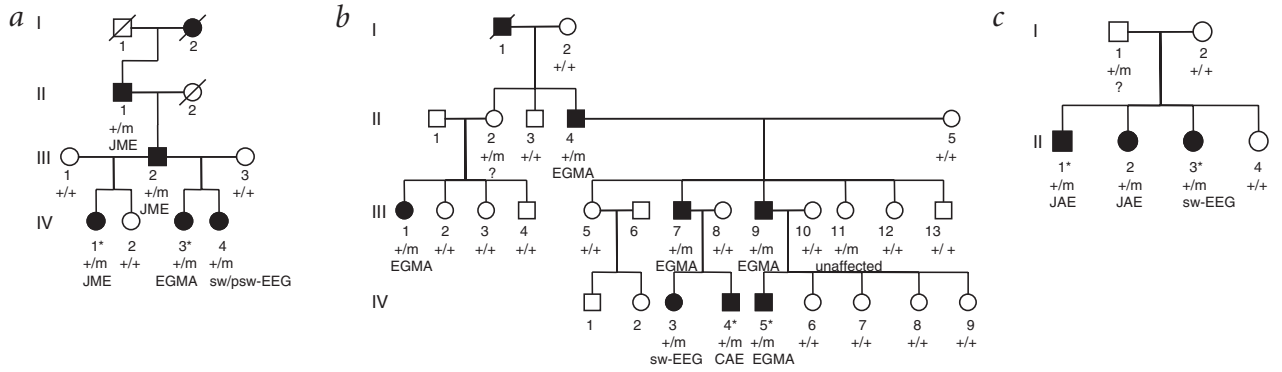

Fig. 1 Segregation analysis of three different mutations in *CLCN2* in families with common IGE subtypes. +/m denotes individuals carrying one of the mutations, and +/+ denotes individuals not carrying the mutation. Asterisks indicate individuals selected for mutation screening. Filled symbols represent individuals diagnosed with JME, JAE, CAE or EGMA. Three individuals were considered affected on the basis of their pathological electroencephalogram showing spontaneous generalized spike-wave (sw-EEG) and/or poly-spike-wave (psw-EEG) discharges. Question marks indicate individuals whose clinical status was unclear. ***a***, Family 1 was identified because individual IV:1 was diagnosed with JME. Segregation analysis showed perfect co-segregation of the mutation 597insG (M200fsX231) and clinical status in this family. ***b***, Individual IV:4 in family 2 experienced daily clusters of absence seizures during childhood (CAE). All affected family members carry the mutation IVS2–14del11 (del74–117), but the occurrence of the mutation in the unaffected individual III:11 indicates incomplete penetrance of this mutation. ***c***, Family 3 was identified because individual II:2 had an epilepsy syndrome that was classified as JAE. All affected family members were found to be heterozygous with respect to the mutation G2144A (G715E).

[1]*Institut für Humangenetik, Universitätsklinikum Bonn, Wilhelmstr. 31, 53111 Bonn, Germany.* [2]*Lehr und Forschungsgebiet Physiologie, RWTH Aachen, 52057 Aachen, Germany.* [3]*Abteilungen für Angewandte Physiologie und Neurologie, Universität Ulm, 89069 Ulm, Germany.* [4]*Neurologische Klinik, Arbeitsgruppe Epilepsie-Genetik, Universitätsklinikum Charité, Campus Virchow Klinikum, Humboldt Universität zu Berlin, Augustenburger Platz 1, 13353 Berlin, Germany.* [5]*Klinik für Epileptologie, Universitätsklinikum Bonn, Sigmund-Freud-Str. 25, 53105 Bonn, Germany.* [6]*Departments of Human Genetics and Biostatistics, University of California, Los Angeles, California, USA.* [7]*Klinik für Pädiatrie, Universitätsklinikum Bonn, Adenauerallee 119, 53113 Bonn, Germany.* [8]*Institut für Biochemie, RWTH Aachen, 52057 Aachen, Germany.* [9]*Centro de Estudios Científicos, Avenida Prat 514, Valdivia, Chile. Correspondence should be addressed to A.H. (e-mail: armin.heils@ukb.uni-bonn.de) or H.L. (e-mail: holger.lerche@medizin.uni-ulm.de).*

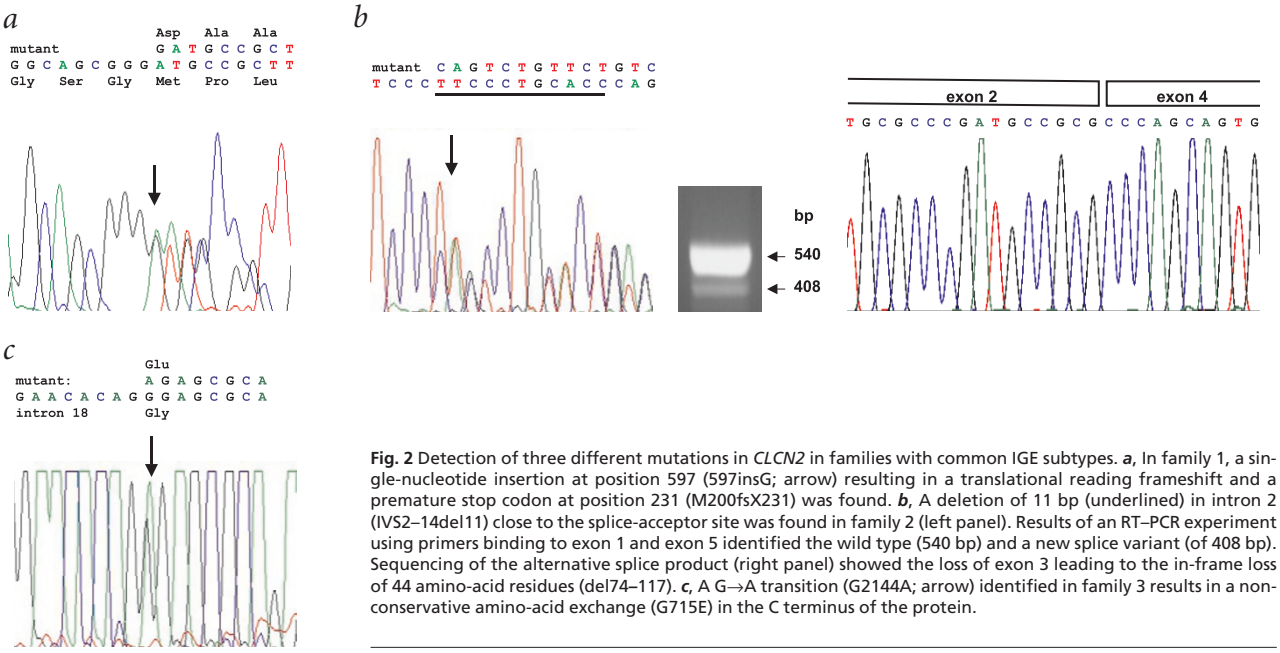

Fig. 2 Detection of three different mutations in *CLCN2* in families with common IGE subtypes. ***a***, In family 1, a single-nucleotide insertion at position 597 (597insG; arrow) resulting in a translational reading frameshift and a premature stop codon at position 231 (M200fsX231) was found. ***b***, A deletion of 11 bp (underlined) in intron 2 (IVS2–14del11) close to the splice-acceptor site was found in family 2 (left panel). Results of an RT–PCR experiment using primers binding to exon 1 and exon 5 identified the wild type (540 bp) and a new splice variant (of 408 bp). Sequencing of the alternative splice product (right panel) showed the loss of exon 3 leading to the in-frame loss of 44 amino-acid residues (del74–117). ***c***, A G→A transition (G2144A; arrow) identified in family 3 results in a non-conservative amino-acid exchange (G715E) in the C terminus of the protein.

Recently, a genome-wide search identified a susceptibility locus for common IGE subtypes on chromosome 3q26 (ref. 9). One of the candidate genes located in this region is *CLCN2*, encoding the voltage-gated chloride channel ClC-2 (refs. 10,11). ClC-2 is strongly expressed in brain, particularly in neurons inhibited by γ-aminobutyric acid (GABA; ref. 12), and has been suggested to have an important role in maintaining a low intracellular chloride concentration ($[Cl^-]_i$) necessary for an inhibitory GABA response[13–15].

We sequenced all 24 exons and adjacent splice sites of *CLCN2* in two affected individuals from 46 unrelated families with IGE. We identified three different heterozygous mutations that co-segregate with common IGE traits in the respective families (Fig. 1). In family 1 (Fig. 1*a*), we detected a single-nucleotide insertion (597insG; Fig. 2*a*), resulting in a premature stop codon (M200fsX231). In family 2 (Fig. 1*b*), we identified a deletion of 11 bp in intron 2 close to the splice-acceptor site, IVS2–14del11 (Fig. 2*b*). RT–PCR using a peripheral blood cell template identified a new splice variant lacking exon 3 (delexon3; Fig. 2*b*), resulting in an in-frame deletion of 44 amino acids (del74–117). Because we found this splice variant in healthy controls also, we established a quantitative competitive RT–PCR assay. In two individuals carrying the IVS2–14del11 mutation, we found 37% less wild-type mRNA and eight times more delexon3 mRNA copies relative to two controls. Accordingly, we found a ratio of delexon3 to wild-type mRNA of 5:95 in controls and of 40:60 in the individuals with the mutation. In family 3 (Fig. 1*c*), we identified the point mutation G2144A (Fig. 2*c*), resulting in the substitution of glutamate for glycine (G715E).

We expressed wild-type, splice variant, and both mutant human ClC-2 channels in tsA201 cells and studied their functional properties using the whole-cell patch–clamp technique. Characteristic current recordings from a cell expressing wild-type ClC-2 (Fig. 3*a*) are shown in Figure 3*b*. The channels activated slowly on membrane hyperpolarization without showing voltage- or time-dependent inactivation. The relative open probability depended

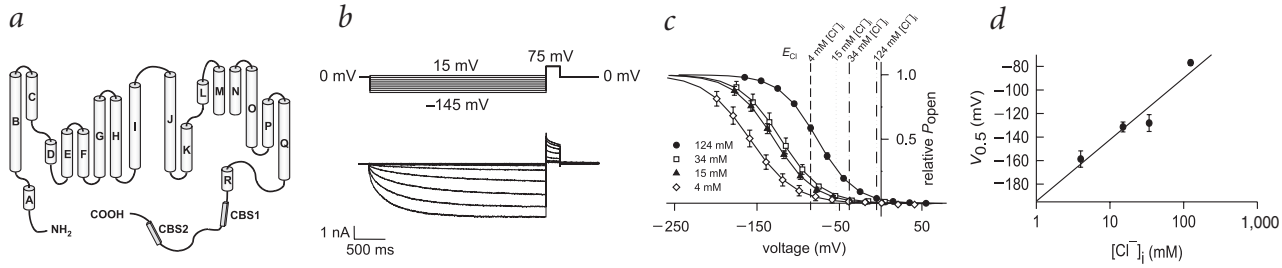

Fig. 3 Gating of wild-type ClC-2 channels depends on the membrane potential and on $[Cl^-]_i$. ***a***, Membrane topology model of ClC-2 (refs. 10,11) based on the high-resolution structure of a ClC channel from *S. typhimurium*[17]. ClC-2 is a polypeptide of 898 amino acids that differs from the prokaryotic isoforms in that it has a cytoplasmic C terminus of 333 amino acids that contains two cystathionine-β-synthase (CBS) domains. ***b***, Voltage-clamp protocol and a typical whole-cell recording from a tsA201 cell expressing wild-type ClC-2 channels. ***c***, Voltage dependence of the relative open probability (P_{open}) of wild-type ClC-2 channels for different internal chloride concentrations ($[Cl^-]_i$). To enable measurements at low $[Cl^-]_i$, the construct wild-type-FCYENE yielding enhanced expression levels was used[28]. Lines represent fits of a standard Boltzmann function to the data points. Midpoints of activation ($V_{0.5}$) at different $[Cl^-]_i$ were as follows: 124 mM, −77 ± 2 mV (n = 10); 34 mM, −128 ± 7 mV (n = 9); 15 mM, −131 ± 4 (n = 7); and 4 mM, −159 ± 7 mV (n = 5). The vertical dashed lines represent the calculated chloride equilibrium potentials (E_{Cl}). ***d***, Midpoint of activation ($V_{0.5}$) as a function of $[Cl^-]_i$ shown as a semi-logarithmic plot (n = 5–10 as in *c*). The line represents a linear regression (r^2 = 0.92). The particular relationship between the midpoint of activation ($V_{0.5}$) and $[Cl^-]_i$ suggests that the voltage dependence of channel opening arises in most part from voltage-dependent binding of intracellular Cl^- (ref. 30).

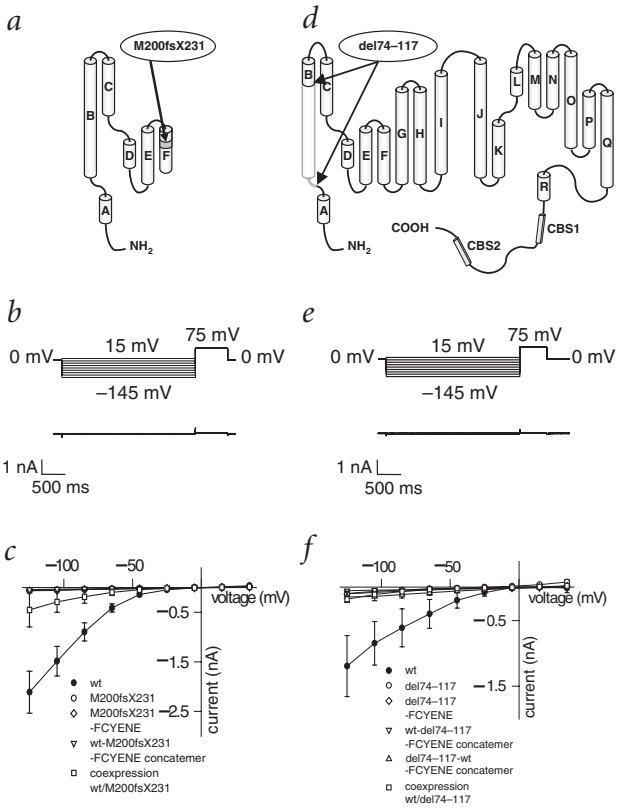

Fig. 4 M200fsX231 and del74–117 cause a loss of function of homo- and heterodimeric mutant channels. ***a***, Proposed topology model for the M200fsX231 mutant ClC-2 channel. ***b***, Voltage-clamp protocol and typical whole-cell recordings from tsA201 cells expressing M200fsX231 mutant ClC-2 channels. There was no detectable current in transfected cells. ***c***, Voltage dependence of averaged peak current amplitudes from cells transfected with wild-type (wt; n = 17), M200fsX231 (n = 12), M200fsX231–FCYENE (n = 4) or wild-type–M200fsX231–FCYENE concatemer (n = 13) or from cells co-transfected with wild-type and M200fsX231 (n = 14). Cells expressing wild-type alone or equal amounts of wild-type and M200fsX231 (co-transfection) were transfected and measured on the same days in parallel. Peak current amplitude for wild-type versus co-transfection of wild-type and M200fsX231 at –125 mV was 2.1 ± 0.4 nA (n = 17) versus 0.5 ± 0.3 nA (n = 14; $P < 0.01$). ***d***, Proposed topology model for the del74–117 splice-variant ClC-2 channel . ***e***, Voltage-clamp protocol and typical whole-cell recordings from tsA201 cells expressing del74–117 mutant ClC-2 channels. There was no detectable current in transfected cells. ***f***, Voltage dependence of averaged peak current amplitudes from cells transfected with wild-type (wt; n = 8), del74–117 (n = 6), del74–117–FCYENE (n = 9), wild-type-del74–117–FCYENE (n = 7) or del74–117–wild-type–FCYENE (n = 7) concatemers or from cells co-transfected with wild-type and del74–117 (n = 8). Cells expressing wild-type alone or equal amounts of wild-type and del74–117 (co-transfection) were transfected and measured on the same days in parallel. Peak current amplitude for wild-type versus co-transfection of wild-type and del74–117 at –125 mV was 1.2 ± 0.5 nA (n = 8) versus 0.2 ± 0.05 nA (n = 8; $P < 0.05$).

on both the membrane potential and the intracellular chloride concentration. Quite similar to native ClC-2 channels in rat hippocampal slices[13], decreasing $[Cl^-]_i$ resulted in a parallel shift of the activation curve to more hyperpolarized potentials (Fig. 3*c*). The particular dependence of gating on $[Cl^-]_i$ ensures that wild-type channels only open at potentials negative to the chloride reversal potential (E_{Cl}; Fig. 3*c*,*d*), thus constituting an exclusive efflux pathway for chloride ions.

The M200fsX231 mutation predicts a truncated protein lacking major sequence determinants of the ionic pore (refs. 16,17; Fig. 4*a*). Heterologous expression of M200fsX231 channels did not yield detectable chloride currents (Fig. 4*b*,*c*). Because ClC channels are dimeric proteins[17,18], we expressed a concatemeric wild-type–M200fsX231 construct and did co-expression experiments. The concatemer was non-functional, and co-transfection with wild-type and mutant cDNAs in a 1:1 ratio resulted in a significantly smaller chloride current than did transfection of wild-type channels alone ($P < 0.01$; Fig. 4*c*).

The splice variant delexon3 predicts the deletion of helix B (ref. 17; del74–117; Fig. 4*d*). Neither this mutant channel nor concatemeric proteins were functional (Fig. 4*e*,*f*). Coexpression experiments showed a dominant negative effect of del74–117 ($P < 0.05$, Fig. 4*f*). Assuming that results from functional studies and quantitative competitive RT–PCR assay are transferable to neurons, we predict more than 60% non-functional channels in individuals carrying the IVS2–14del11 mutation as compared with less than 10% non-functional channels in controls.

We examined the subcellular localization of non-functional proteins using constructs tagged with yellow fluorescent protein (YFP). In all cases, we observed fluorescence in the plasma membrane (Fig. 5). This indicates that the loss of function and the dominant negative effect were not due to altered channel trafficking but to impaired channel function.

In contrast to M200fsX231 and del74–117, G715E mutant channels were functional and had normal current amplitudes but altered voltage-dependent gating (Fig. 6). At $[Cl^-]_i$ of 4, 15 and 34 mM, the voltage dependence of activation of G715E mutant channels was shifted to more positive potentials compared with wild-type channels ($P < 0.05$; Figs. 3*c*,*d* and 6*c*,*d*), causing mutant channels to open at less negative potentials in a physiological chloride range. Heterodimeric wild-type–G715E channels had an intermediate voltage dependence as deduced from coexpression experiments (see legend to Fig. 6).

Wild-type hClC-2 channels act as a chloride-efflux pathway well suited to establishing and maintaining a high transmembrane Cl^- gradient necessary for an inhibitory GABA response. Owing to the coupling of channel activation to $[Cl^-]_i$ and the slow gating, they are closed under resting conditions and during action potentials or isolated excitatory postsynaptic potentials. They open with long-lasting changes of the transmembrane Cl^- gradient when E_{Cl} becomes more positive than the membrane potential[13] (for example, when $[Cl^-]_i$ is increased after intense

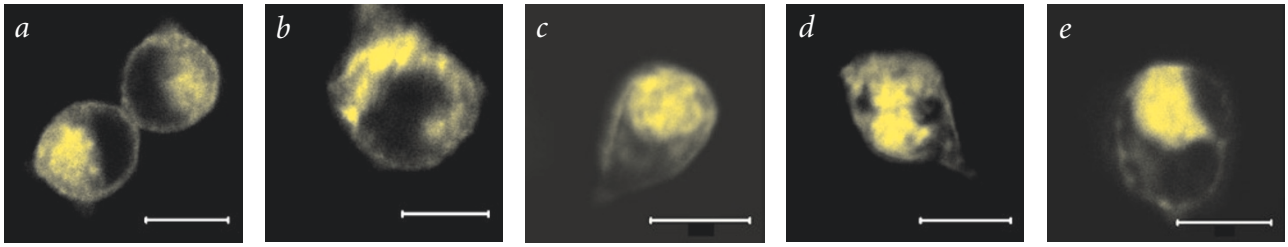

Fig. 5 Non-functional mutants are inserted into the cell membrane. Fluorescence signals of YFP-tagged wild-type (***a***), M200fsX231 (***b***) and del74–117 (***c***) channels and of the concatemeric constructs wild-type–M200fsX231 (***d***) and wild-type–del74–117 (***e***) were detected using a confocal laser scanning microscopy. Scale bars = 10 μm.

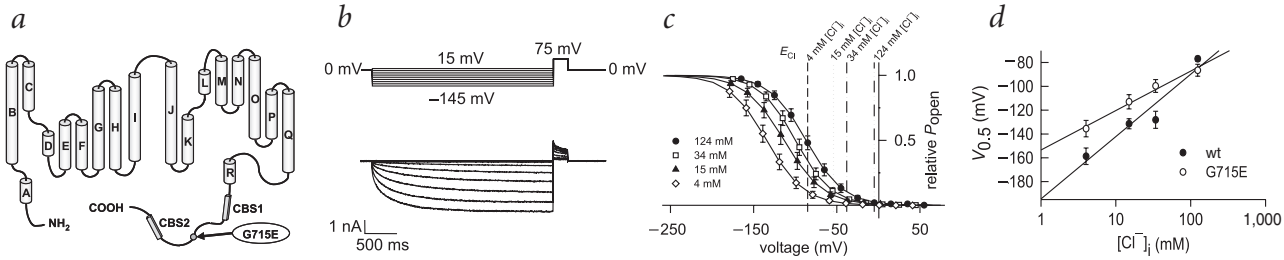

Fig. 6 The G715E mutation alters the chloride dependence of ClC-2 gating. ***a***, Proposed topology model of ClC-2 showing the position of the point mutation G715E in the intracellularly located C terminus of the channel. ***b***, Voltage-clamp protocol and a typical whole-cell recording from a tsA201 cell expressing G715E mutant ClC-2 channels. ***c***, Voltage dependence of P_{open} of G715E–ClC2–FCYENE channels (compare with Fig. 3*c*). $V_{0.5}$ at different $[Cl^-]_i$ were as follows: 124 mM, –87 ± 5 mV (n = 7); 34 mM, –100 ± 5 mV (n = 4; P < 0.05 compared to wild-type); 15 mM, –113 ± 6 mV (n = 8; P < 0.05 compared to wild-type); and 4 mM, –136 ± 7 mV (n = 8; P < 0.05 compared to wild-type). Vertical lines represent E_{Cl} as in Figure 3c. Co-expression of wild-type and G715E mutant channels was done at $[Cl^-]_i$ of 15 mM and showed an intermediate $V_{0.5}$ of –123 ± 9 mV (n = 6; results not shown). These data did not differ significantly from either wild-type or G715E monomeric channels. ***d***, Midpoint of activation ($V_{0.5}$) as a function of $[Cl^-]_i$ shown as a semilogarithmic plot for wild-type (wt; filled circles) and G715E (open circles) as in Figure 3*d* (n = 4–10). Lines represent linear regressions (wild-type, r^2 = 0.92; G715E, r^2 = 0.98). The distinct dependence of $V_{0.5}$ on $[Cl^-]_i$ suggests that G715E channels have a higher K_D (at 0 mV) and a steeper voltage dependence of Cl^- binding than do wild-type channels[30].

GABAergic inhibition[19]) and extrude chloride until E_{Cl} approaches the resting membrane potential.

A passive transport mechanism by a channel-mediated chloride flux is, however, by itself unable to generate an E_{Cl} more negative than the resting membrane potential, as observed in many neurons. It is well established that an outwardly directed coupled transport of K^+ and Cl^- by the neuron-specific KCC2 transporter is necessary in generating the low $[Cl^-]_i$ essential for GABAergic inhibition[19–21]. K–Cl cotransport by KCC2 is driven by the transmembrane K^+ gradient and causes Cl^- extrusion near the resting potential[19,20]. Increases of $[K^+]_o$, such as induced by high-frequency activity of GABAergic interneurons[22], affect the rate and the direction of this transport[19,23]. This can cause impaired Cl^- extrusion or even inward K–Cl cotransport by KCC2 (refs. 19,20,22,23). Under these conditions, ClC-2 seems to be the primary chloride extrusion pathway to reestablish a negative E_{Cl} and preserve an inhibitory GABA response. An impaired chloride efflux in neurons of individuals carrying the 597insG or the IVS2–14del11 mutation should thus result in intracellular chloride accumulation. Consequently, the inhibitory GABA response would be reduced or might even become excitatory, resulting in neuronal hyperexcitability and epileptic seizures.

The G715E mutation seems to cause neuronal hyperexcitability by a distinct mechanism. After intense synaptic activity causing membrane depolarization by activation of glutamate receptors and Cl^- influx through $GABA_A$ receptors, G715E mutant channels conduct an increased outward Cl^- current during repolarization after passing E_{Cl}. Quite analogous to pacemaker channels in heart and brain, this abnormal conductance may induce recurrent membrane depolarization beyond action potential threshold. This gain of function would cause the postsynaptic membrane of GABAergic synapses to become hyperexcitable and could thus induce epileptic seizures in heterozygous individuals. In contrast, the particular chloride dependence of wild-type channels might prevent substantial depolarization by keeping the Cl^- efflux at a low level.

A recently reported *Clcn2*-knockout mouse model did not have epileptic seizures[24]. But mouse models often differ from human diseases. For example, transgenic mice with either a knockout or 'knock-in' of *Chrna4*, expected to be an animal model for autosomal dominant nocturnal frontal lobe epilepsy (ADNFLE; refs. 1,2), were not reported to develop seizures[25,26]. Compensatory mechanisms that are distinct in humans and mice, as well as characteristic anatomical and physiological properties, may account for these species-specific differences.

We idnetified *CLCN2* to be associated with pure forms of the four most common IGE subtypes, which are considered genetically complex traits[27]. The mutations in *CLCN2* that we report here confer a major gene effect that seems to lead to a monogenic disease in affected families. But distinct predominant clinical phenotypes in these families suggest that unidentified genes or distinct genetic backgrounds may also be important, which is compatible with a complex rather than monogenic mode of inheritance. Most clinically affected individuals experienced generalized tonic-clonic seizures (GTCSs), which is in agreement with a generally high prevalence of GTCSs in common IGE syndromes. Nevertheless, the possibility that mutations in *CLCN2* may confer greater susceptibility to GTCSs regardless of the underlying IGE syndrome cannot be excluded.

We identified only three mutations in a total of 46 selected families sharing common marker haplotypes at 3q26. Other unidentified mutations may be localized in regulatory or intronic regions of *CLCN2* or in other genes at this locus (except for *KCNAB1*, *KCNMB3* and *KCNMB2*, which we excluded in our sample by means of systematic mutation screening and association studies; data not shown). Also, common marker haplotypes at 3q26 in affected individuals could have occurred by chance, particularly in small families, and might not necessarily be associated with a mutation in this chromosomal region.

All the mutations that we identified in *CLCN2*, albeit by distinct mechanisms, predict a hyperexcitability of the postsynaptic membrane of GABAergic synapses. These findings, together with the recent identification of mutations in two different genes encoding $GABA_A$ receptor subunits in families with idiopathic epilepsies[4,5,7], provide further evidence for an important role of a genetically driven dysfunction of GABAergic inhibition in epileptogenesis.

Methods

Study sample selection and family histories. A recent genome-wide linkage study[9] included 130 families affected with IGE who had been identified through an international consortium of numerous research groups. This study[9] provided significant evidence for the chromosome 3q26 susceptibility locus. We collected samples from 55 of these 130 families at one of the participating clinical centers of this study (in Berlin) and from 42 other families with IGE in Bonn. We carried out a systematic search for mutations in *CLCN2* in 46 families with IGE (Berlin, n = 23; Bonn, n = 23) in which linkage to chromosome 3q26 could not be excluded by means of affected individuals sharing common marker haplotypes (IBD-segment sharing). In these families, two-point linkage analysis assuming an autosomal dominant mode of inheritance gave rise to a cumulative lod score of 11.47 at the marker *D3S3730* closest to *CLCN2*. The three families in whom

we found mutations had an overall lod score of 4.66.

Diagnostic classification was done by experienced neurologists following standard criteria[8]. We obtained EEG recordings from all affected individuals and also from clinically unaffected family members, and these were analyzed by neurologists who were unaware of the clinical diagnosis of the individuals. We considered individuals to be affected when they presented with either a history of primary generalized seizures or an EEG pattern typical for IGE, such as spontaneous generalized spike and wave or polyspike-wave discharges. The study was approved by the local Ethics Committees of the participating centers and written informed consent was obtained from all participants.

In family 1 (Fig. 1*a*), the most common IGE syndrome was JME, but individual IV:3 was diagnosed with EGMA. All clinically affected family members experienced frequent GTCSs. Myoclonic jerks often occurred in a series finally followed by GTCSs. Affected individuals became seizure-free only when treated with high dosages of valproate in combination with other antiepileptic drugs. In family 2 (Fig. 1*b*), all affected family members except individual IV:4 experienced no more than two or three GTCSs on awakening, and these individuals became seizure-free without requiring antiepileptic medication. Individual IV:4 presented with CAE with typical pyknoleptic daily clusters of absence seizures at the age of four years. The child became seizure-free when treated with valproate. In family 3 (Fig. 1*c*), we diagnosed two affected siblings with JAE. Individual II:1 experienced spanioleptic absence seizures at the age of 11 years followed by few unprovoked GTCSs at the same age. His sister (individual II:2) was diagnosed with JAE also at the age of 11 years, presenting with isolated absence seizures. At the age of 19 years, she also experienced few GTCSs. Both clinically affected family members, as well as their clinically unaffected sister (individual II:3), showed spontaneous generalized spike-wave discharges. The father was reported to have had unclassifiable seizures since childhood, but, as he now suffers from severe alcoholism probably accounting for his present GTCSs, he was classified with an unclear clinical status. In all three families, one individual was regarded as affected based on unprovoked generalized epileptiform discharges in the EEG.

Mutation screening. We determined the genomic organization of *CLCN2* by comparing the published cDNA sequence with a genomic human chromosome 3 BAC clone. We identified 24 coding exons and adjacent intronic sequences, which allowed us to create primers for the amplification of all coding exons (primer sequences are available on request). For mutation screening, we directly sequenced (using an ABI 377 automated sequencer) all coding exons and adjacent splice sites from genomic DNA of two affected family members from each of the 46 families included in this study. We then excluded the presence of each mutation that we identified in a sample consisting of 180 ethnically matched controls (360 control chromosomes).

RT–PCR and quantitative competitive RT–PCR. We identified the delexon3 splice variant by standard RT–PCR (primer sequences are available on request) and direct sequencing of respective PCR products.

To determine the relative amount of variant and wild-type *CLCN2* mRNA in peripheral blood cells from two individuals carrying the IVS2–14del11 mutation (individuals III:7 and IV:4), one family member carrying two wild-type alleles (individual III:5; Fig. 1*b*) and one independent unaffected control subject, we established a quantitative competitive RT–PCR assay. We extracted total RNA from EDTA-anticoagulated blood samples using the Qiamp RNA Blood Mini Kit (Qiagen) according to the manufacturer's instructions. We determined the concentrations of total RNA prepared by A_{260} and adjusted the concentrations by semiquantitative RT–PCR using the human hypoxanthine phosphoribosyltransferase 1 (*HPRT1*) transcript as an internal standard. We generated competitors for mutated and wild-type *CLCN2* in the pCR2.1-TOPO vector (Invitrogen) and introduced a 91-bp internal deletion in both competitors by standard recombinant PCR technology to produce PCR products of different lengths.

For quantitative competitive RT–PCR, we generated target-specific primer sets binding to either the wild-type or the mutated cDNA (primer sequences are available on request). We did serial tenfold dilutions of competitor DNAs and added these to RT–PCR tubes. We carried out one-tube quantitative competitive RT–PCR under the following conditions: reverse transcription at 50 °C for 30 min; 95 °C for 15 min; 23 identical cycles of denaturation (94 °C for 30 s), annealing (68 °C for 20 s) and extension (72 °C for 1 min); and a final extension of 5 min at 72 °C. We separated products of quantitative competitive RT–PCR on a 2% agarose gel. We analyzed and quantified the band intensities using an image processing system (Gel-doc 1000 camera system and image analysis software; molecular analysis software, Bio-Rad Lab). We calculated the relative amounts of wild-type and mutated *CLCN2* cDNA in two individuals carrying the IVS2–14del11 mutation and in two controls by determining the equivalent point in a logarithmic linear regression plot using mean values of five independent experiments in each individual.

Plasmid construction, mutagenesis and transfection. We introduced an N-terminal *Not*I restriction site by PCR into a full length *CLCN2* cDNA in plasmid pBK/RSV (ref.11; Invitrogen). We then subcloned this construct into pcDNA3.1 (Invitrogen). To increase expression levels, we introduced an endoplasmic reticulum export signal (FCYENE; ref. 28) at the C terminus of *CLCN2* and created an additional C-terminal *Xba*I restriction site to subclone this construct into pRc/CMV (Invitrogen). We introduced the mutations into both constructs using PCR-based techniques and verified the correct insertion by sequencing. For wild-type and all mutations, constructs with and without FCYENE had indistinguishable biophysical properties. We constructed plasmids to express channels tagged with YFP by creating a *Not*I restriction site at the C terminus of the coding region of YFP in pEYFP-N1 (Clontech) and ligating an *Age*I/*Not*I fragment into various pRcCMV–*CLCN2* constructs. Transfection of these constructs caused the expression of covalently linked YFP-channel constructs. We carried out transient transfection of tsA201 cells using the $Ca_3(PO_4)_2$ technique as previously described[29]. For each mutation, we examined at least two independent recombinants.

We designed concatemeric constructs linking two wild-type or one mutant and one wild-type *CLCN2* sequence in a single open reading frame as described previously for *CLCN1* (ref. 29). Transfection of concatemeric wild-type–wild-type constructs in tsA201 cells resulted in peak current amplitudes comparable with those observed from monomeric wild-type constructs. For M200fsX231, the wild-type sequence was located 5′ to the mutant sequence. For the splice variant, we examined both wild-type–del74–117 and del74–117–wild-type concatemers. G715E–G715E concatemers had distinct gating properties from those of G715E monomeric constructs. Therefore, we did not use wild-type–G715E concatemers to study functional properties of heterodimeric channels. Co-expression of wild-type and G715E channels showed results intermediate between those for wild-type and G715E monomeric channels (Fig. 6*c*). But the voltage dependence of activation obtained from co-transfected cells represents the sum of three distinct Boltzmann functions for wild-type–wild-type, wild-type–G715E and G715E–G715E channels, respectively, and it was not possible to extract properties of pure wild-type–G715E heterodimeric channels.

We carried out co-transfections of wild-type and mutant *CLCN2* in a 1:1 ratio of transfected cDNA. To examine a possible dominant negative effect of M200fsX231 and del74–117 on the wild-type, we transfected the cells on the same day with either wild-type alone or the same amount of wild-type plus the same amount of mutated cDNA.

Electrophysiological recordings. We did standard whole-cell patch–clamp recordings as described[29]. The standard extracellular (bath) solution contained 140 mM NaCl, 4 mM KCl, 2 mM $CaCl_2$, 1 mM $MgCl_2$ and 5 mM HEPES buffer, pH 7.4. We composed four intracellular (pipette) solutions with different $[Cl^-]_i$ (compositions of these solutions are available on request). We used agar bridges to connect the bath solution and, when the intracellular solution contained glutamate, also the pipette solution to the amplifier. Between voltage steps, we held the cells to potentials close to the calculated chloride equilibrium potential. We used junction potentials calculated by the JPCalc software (P. Barry) to correct results.

To determine the voltage dependence of activation, we measured the instantaneous current amplitude 200 µs after a voltage step to 75 mV after test pulses to different voltages (V), normalized it to its maximum value and plotted it versus the test potential. To reach steady-state conditions, we adjusted the test pulse duration to 2.5 s. Steady-state activation curves obtained in this manner were fit using a single Boltzmann function plus a constant term: $I(V) = A/(1 + \exp(V - V_{0.5})/k_V) + C$, where $I(V)$ represents the voltage-dependent current amplitude; A, an amplitude factor; $V_{0.5}$, the voltage of half-maximal activation; k_V, a slope factor; and C, a constant term. After subtracting the leak current component C, we divided current amplitudes by A to obtain the relative steady-state open probability of ClC-2 (Figs. 3 and 6). We analyzed the data using a combination of pClamp (Axon Instruments) and SigmaPlot

(Jandel Scientific) programs. For statistical evaluation we used Student's *t*-test. All data are shown as mean ± s.e.m.

Confocal microscopy. We grew transfected tsA201 cells on coverslips, fixed them with formaldehyde 48 h after transfection and mounted them with Mowiol (Calbiochem). We took confocal images using a Zeiss LSM 510 confocal microscope equipped with a 63× water-corrected Plan-Apochromat objective. Yellow fluorescent protein was excited with the 514-nm line of the argon ion laser. For detection of fluorescence we used a >530-nm long-pass filter.

GenBank accession numbers. *Homo sapiens CLCN2* mRNA, NM_004366; *Homo sapiens* 3 BAC RP11-125E8, AC078797.

Acknowledgments

The authors thank all affected individuals and their families who participated in this study; H. Beck, F. Lehmann-Horn, J.P. Johnson and A. Ryan for discussion on the manuscript; P.C. Heinrich for support; and G. Cutting for providing the pBKRSV-hClC-2 construct. This work was supported by the German Volkswagen-Stiftung (to A.H.), the Deutsche Forschungs-Gemeinschaft (to A.H., C.F., H.L. & T.S.), the German Bundesministerium für Bildung und Forschung (to A.H. & H.L.), the Stiftung Michael (to T.S.), BONFOR (to A.H.) and the Muscular Dystrophy Association (to C.F.).

Competing interests statement

The authors declare that they have no competing financial interests.

Received 13 September 2002; accepted 30 January 2003.

1. Steinlein, O.K. & Noebels J.L. Ion channels and epilepsy in man and mouse. *Curr. Opin. Genet. Dev.* **10**, 286–291 (2000).
2. Berkovic, S.F. & Scheffer, I.E. Genetics of the epilepsies. *Epilepsia* **42**, Suppl 5 16–23 (2001).
3. Lerche, H., Jurkat-Rott, K. & Lehmann-Horn, F. Ion channels and epilepsy. *Am. J. Med. Genet.* **106**, 146–159 (2001).
4. Baulac, S. *et al.* First genetic evidence of $GABA_A$ receptor dysfunction in epilepsy: a mutation in the γ2-subunit gene. *Nat. Genet.* **28**, 46–48 (2001).
5. Wallace, R.H. *et al.* Mutant $GABA_A$ receptor γ2-subunit in childhood absence epilepsy and febrile seizures. *Nat. Genet.* **28**, 49–52 (2001).
6. Kalachikov, S. *et al.* Mutations in *LGI1* cause autosomal-dominant partial epilepsy with auditory features. *Nat. Genet.* **30**, 335–341 (2002).
7. Cossette, P. *et al.* Mutation of *GABRA1* in an autosomal dominant form of juvenile myoclonic epilepsy. *Nat. Genet.* **31**, 184–189 (2002).
8. Commission on Classification and Terminology of the International League Against Epilepsy. Proposal for revised classification of epilepsies and epileptic syndromes. *Epilepsia* **30**, 389–399 (1989).
9. Sander, T. *et al.* Genome search for susceptibility loci of common idiopathic generalized epilepsies. *Hum. Mol. Genet.* **9**, 1465–1472 (2000).
10. Thiemann, A., Gründer, S., Pusch, M. & Jentsch, T.J. A chloride channel widely expressed in epithelial and non-epithelial cells. *Nature* **356**, 57–60 (1992).
11. Cid, L.P., Montrose-Rafizadeh, C., Smith, D.I., Guggino, W.B. & Cutting, G.R. Cloning of a putative human voltage-gated chloride channel (ClC-2) cDNA widely expressed in human tissues. *Hum. Mol. Genet*. **4**, 407–413 (1995).
12. Sik, A., Smith, R.L. & Freund, T.F. Distribution of chloride channel-2-immunoreactive neuronal and astrocytic processes in the hippocampus. *Neuroscience* **101**, 51–65 (2000).
13. Staley, K.J. The role of an inwardly rectifying chloride conductance in postsynaptic inhibition. *J. Neurophysiol.* **72**, 273–284 (1994).
14. Mladinic, M., Becchetti, A., Didelon, F., Bradbury, A. & Cherubini, E. Low expression of the ClC-2 chloride channel during postnatal development: a mechanism for the paradoxical depolarizing action of GABA and glycine in the hippocampus. *Proc. R. Soc. Lond. B Biol. Sci.* **266**, 1207–1213 (1999).
15. Staley, K.J., Smith, R., Schaack, J., Wilcox, C. & Jentsch, T.J. Alteration of $GABA_A$ receptor function following gene transfer of the ClC-2 chloride channel. *Neuron* **17**, 543–551 (1996).
16. Fahlke, C., Yu, H.T., Beck, C.L., Rhodes, T.H. & George, A.L.Jr. Pore-forming segments in voltage-gated chloride channels. *Nature* **390**, 529–532 (1997).
17. Dutzler, R., Campbell, E.B., Cadene, M., Chait, B.T. & MacKinnon, R. X-ray structure of a ClC chloride channel at 3.0 A reveals the molecular basis of anion selectivity. *Nature* **415**, 287–294 (2002).
18. Miller, C. Open-state substructure of single chloride channels from Torpedo electroplax. *Philos. Trans. R. Soc. Lond. B Biol. Sci.* **299**, 401–411 (1982).
19. Thompson, S.M. & Gähwiller, B.H. Activity-dependent disinhibition II: Effects of extracellular potassium, furosemide, and membrane potential on E_{Cl} in hippocampal CA3 neurons. *J. Neurophysiol.* **61**, 512–523 (1989).
20. Misgeld, U., Deisz, R.A., Dodt, H.U. & Lux, H.D. The role of chloride transport in postsynaptic inhibition of hippocampal neurons. *Science* **232**, 1413–1415 (1986).
21. Rivera, C. *et al.* The K^+/Cl^- co-transporter KCC2 renders GABA hyperpolarizing during neuronal maturation. *Nature* **397**, 251–255 (1999).
22. Kaila, K., Lamsa, K., Smirnov, S., Taira, T. & Voipio, J. Long-lasting GABA-mediated depolarization evoked by high-frequency stimulation in pyramidal neurons of rat hippocampal slice is attributable to a network-driven, bicarbonate-dependent K^+ transient. *J. Neurosci.* **17**, 7662–7672 (1997).
23. Payne, J.A. Functional characterization of the neuronal-specific K–Cl cotransporter: implications for $[K^+]_o$ regulation. *Am. J. Physiol.* **273**, C1516–C1525 (1997).
24. Bösl, M.R. *et al.* Male germ cells and photoreceptors, both dependent on close cell-cell interactions, degenerate upon ClC-2 Cl^- channel disruption. *EMBO J.* **20**, 1289–1299 (2001).
25. Ross, S.A. *et al.* Phenotypic characterization of an α_4 neuronal nicotinic acetylcholine receptor subunit knock-out mouse. *J. Neurosci.* **20**, 6431–6441 (2000).
26. Labarca, C. *et al.* Point mutant mice with hypersensitive α_4 nicotinic receptors show dopaminergic deficits and increased anxiety. *Proc. Natl. Acad. Sci. USA* **98**, 2786–2791 (2001).
27. Serratosa, J.M. Idiopathic epilepsies with a complex mode of inheritance. *Epilepsia* **40**, 12–16 (1999)
28. Ma, D. *et al.* Role of ER export signals in controlling surface potassium channel numbers. *Science* **291**, 316–319 (2001).
29. Fahlke, C., Knittle, T., Gurnett, C.A., Campbell, K.P. & George, A.L.Jr. Subunit stoichiometry of human muscle chloride channels. *J. Gen. Physiol.* **109**, 93–104 (1997).
30. Cui, J., Cox, D.H. & Aldrich, R.W. Intrinsic voltage dependence and Ca^{2+} regulation of mslo large conductance Ca^{2+}-activated K^+ channels. *J. Gen. Physiol.* **109**, 647–673 (1997).

Retraction: Mutations in *CLCN2* encoding a voltage-gated chloride channel are associated with idiopathic generalized epilepsies

Karsten Haug, Maike Warnstedt, Alexi K Alekov, Thomas Sander, Alfredo Ramírez, Barbara Poser, Snezana Maljevic, Simon Hebeisen, Christian Kubisch, Johannes Rebstock, Steve Horvath, Kerstin Hallmann, Joern S Dullinger, Birgit Rau, Fritz Haverkamp, Stefan Beyenburg, Herbert Schulz, Dieter Janz, Bernd Giese, Gerhard Müller-Newen, Peter Propping, Christian E Elger, Christoph Fahlke, Holger Lerche & Armin Heils

***Nat. Genet.* 33, 527–532 (2003); published online 3 March 2003**

Re-examination of the families and the molecular genetic data by a neurologist and a geneticist who were not involved in the original study has revealed major differences from the published data in two of the three published pedigrees (presented in Figs. 1a,b of the original publication). The number of clinically affected individuals was much lower than was previously reported, and large parts of the pedigree structures and epilepsy phenotypes are different. Most importantly, re-examination revealed the existence of several asymptomatic mutation carriers, refuting the complete co-segregation of the two mutations with the clinical phenotypes that was originally reported. A detailed description of these differences, including the clinical phenotypes and the genetic reanalysis, is provided in the related Correspondence in this issue[1].

We sincerely regret our failure to recognize that important family data were false before the original manuscript was published, and we apologize for any inconvenience that may have arisen as a result of our report.

A. Heils did not agree to coauthor this retraction.

1. Kleefuß-Lie, A. *et al. Nat. Genet.* **41**, 954–955 (2009).